



Energy mass balance and temperature-index melt modelling of Werenskioldbreen, Svalbard

Dariusz IGNATIUK 

University of Silesia in Katowice, Bankowa 12, 40-007 Katowice, Poland

<dariusz.ignatiuk@us.edu.pl>

Abstract: Studying the reaction of glaciers to climate warming and the interactions of ice masses with the atmosphere is cognitively highly significant and contributes to understanding the climate change. The results from the modelling of glacier surface ablation by the temperature–index and energy balance models as well as the results of meteorological and glaciological studies on Werenskioldbreen (south Spitsbergen, Svalbard) in 2011 have been analysed to improve the understanding of the glacier system’s functioning in the High Arctic. The energy balance modelling results showed that the radiation balance (58%) and sensible heat (42%) are the main factors influencing surface ablation on the glacier. The energy balance model offers a better fit to the measured ablation than the temperature–index model. These models have to be validated and calibrated with data from automatic weather stations, which provide the relevant gradient and calibration and validation. Presented models are highly suited for calculating ablation in Svalbard and other areas of the Arctic.

Keywords: Arctic, Spitsbergen, degree-day factor, melt modelling, glacier mass balance.

Introduction

The melting of continental ice is making a considerable contribution to ongoing sea-level rise and has been one of the factors accelerating this process in recent years. According to the 2019 Report by the Intergovernmental Panel on



Climate Change (IPCC 2019), inaccuracies in forecasting future sea-level changes are dominated by errors in estimating runoff from ice masses and incomplete understanding of the key processes that are leading to their disappearance. Studying the reaction of glaciers to climate warming and the interactions of ice masses with the atmosphere is significant in analysing climate change trends. Thus, the results of this basic research have practical consequences in the Arctic, as well as for temperate latitudes.

An unmistakable indicator of the changes taking place in the Atlantic part of the Arctic is the evolution of glaciers on Svalbard, which has been observed since the beginnings of the 20th century (Błaszczuk *et al.* 2013, 2021; Nuth *et al.* 2019; Van Pelt *et al.* 2019; Schuler *et al.* 2020). This evolution is manifested by changes in the hydrothermal structure of the glaciers taking place as a result of climate change and changes in their dynamics. Climate changes affect the energy balance of the glacier surface, and hence, the magnitude of ablation. The presence of liquid water within, on the surface of and under the ice is of immense importance in many glacial processes. The speed with which a glacier slides over its substrate to a large extent depends on the pressure of subglacial waters (Paterson 1994). Meltwaters are the main mechanism by which ice mass is lost. In most cases, the principal source of water in a glacier is surface melting, the rate of which is governed by the energy balance of its surface. Other sources of water may be inflows of water from non-glaciated slopes in the vicinity of the glacier, waters formed at the glacier-substrate interface, ice-dammed lakes or rainfall.

In a view of the difficulties in direct measuring the volumes of meltwaters forming on the surface of a glacier, the indirect method of modelling the energy balance may offer a more practical approach to the problem of melting and thus the flow of meltwaters into the body of the glacier. Energy balance modelling is completed for various kinds of terrain surface, including glaciated areas (Hock 1998). The few papers addressing the problem of the energy balance of Svalbard glaciers are generally based partly on field measurements and partly on extrapolating data from weather stations, which can be as far away as 60 km away (Den Ouden *et al.* 2008). Results obtained in this way are hindered with error resulting from the fact that the local climate, which mediates the real hydrothermal conditions in glaciers, is not accounted for. The present paper discusses modelling based on data acquired in situ on the glacier to be modelled. The aims of this study are to develop energy balance model of glacier surface, to identify the main factors influencing the energy balance and to determine the impact of the major components of this balance in the ablation processes on the example of Werenskioldbreen.

Research of this type, performed hitherto on Svalbard, has usually related to small glaciers like Midre Lovénbreen (Hodson *et al.* 2005), and the results are not entirely representative for entire Svalbard. The only attempts undertaken so far at modelling the mass balance of Werenskioldbreen, a medium size glacier, were based on correlations with meteorological observations and data from climate re-analysis (Grabiec *et al.* 2012).

Study area

Werenskioldbreen is a polythermal glacier situated in Wedel-Jarlsberg Land, South Spitsbergen (Fig. 1). Its catchment area of 44 km² contains a valley-type glacier that covered an area of 27.1 km² in 2008 (Ignatiuk *et al.* 2015) and 25.7 km² in 2017 (Ignatiuk *et al.* 2022). The mean retreat rate between 1957 and 2019 was *c.* 25 m/year (Cieżykowski *et al.* 2018).

Werenskioldbreen is well-studied, which, together with its forefield and river gorge, served as a well-defined research laboratory for glaciological (Baranowski 1982; Pälli *et al.* 2003; Grabiec *et al.* 2012; Ignatiuk *et al.* 2015, 2022), hydrological (Majchrowska *et al.* 2015; Stachnik *et al.* 2016a, 2016b, 2022; Łepkowska and Stachnik 2018; Osuch *et al.* 2022) and interdisciplinary studies (Gwizdała *et al.* 2018; Sułowicz *et al.* 2020).

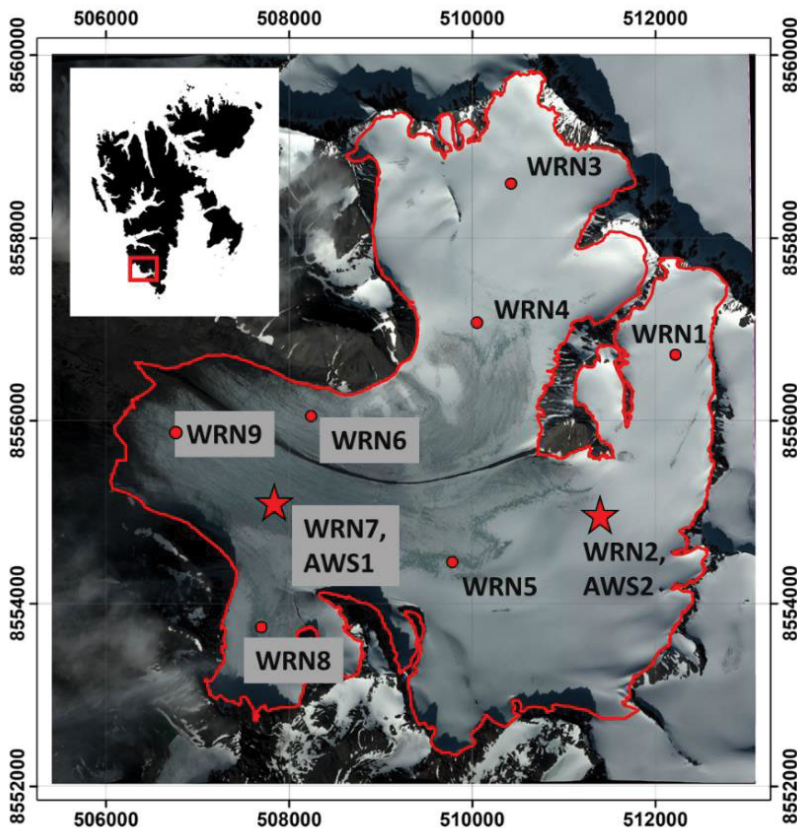


Fig. 1. Locations of the automatic weather stations AWS1 and AWS2 as well as mass-balance stakes (WRN1 to WRN9) in 2011 on Werenskioldbreen (background: GeoEye-1 VHRS image acquired on 10 August 2010).

Methods and models

Meteorological and glaciological monitoring. — The first automatic weather station (AWS1) was located at altitude of 230 m a.s.l. (UTM 33N, N8555045; E507837) and the second (AWS2) at altitude of 380 m a.s.l. (UTM 33N, N8555045; E510423) (Fig. 1). AWS2, the main meteorological station, was equipped with temperature (107/Campbell Scientific), humidity (HOBO) and wind speed (A100R) sensors on two levels at a vertical distance of 1.5 m from each other. At this station, a Kipp & Zonen CNR4 sensor consisting of two CM3 pyranometers, two CG3 pyrgeometers and temperature sensors (PT100) were installed for radiation balance measurements. Changes in snow depth and ice ablation were recorded using an ultrasonic sensor SR50/SR50A (Campbell Scientific). This sensor utilizes a 50 kHz acoustic signal, applied with a temperature correction, and records the distance between the ground and the sensor level. A Schlumberger Baro-Diver sensor was installed for air pressure measurements, for more details about AWS2 see Ignatiuk *et al.* (2022). Data from AWS1 were used to determine the spatial variability of air temperature on the glacier and to validate the models. It was also equipped with two temperature sensors (107/Campbell Scientific) installed on two levels at a vertical distance of 1.5 m from each other. In addition, the temperature was measured every 0.25 m to a depth of 1 m from the glacier surface using four PT-107 sensors installed in the snow cover.

For the glaciological monitoring, nine mass-balance stakes WRN1 to WNR9 were installed (Fig. 1). The spatial distribution of the stakes covered the altitude range from 117 m to 515 m a.s.l., thus ensuring good coverage of the spatial accumulation and ablation data. During the period analysed, the stakes were measured twice a year: in September–October, at the end of the ablation season, and in April–May, during the maximum winter accumulation (Ignatiuk *et al.* 2022). All the data and detailed parameters of the meteorological and glaciological monitoring can be found in the Zenodo data repository (Ignatiuk 2021a, 2021b; Ignatiuk *et al.* 2022).

Temperature index model. — The temperature index model is founded on the relationship between the glacier surface ablation and positive daily temperatures. The annual ablation is highly correlated (0.96) with the sum of positive daily air temperatures (Braithwaite and Olsen 1989) owing to the strong dependence of the air temperature on the components of the energy balance (Hock 2003). Ohmura (2001) discussed the physical basis for applying temperature ablation models, the relationship between air temperature and longwave radiation of the atmosphere, sensible heat and incident shortwave radiation. The temperature index model is given by the equation after Braithwaite (1995):

$$\sum_{i=1}^n M = DDF \sum_{i=1}^n T^+ \Delta t \quad (1)$$

$$DDF = \frac{M_m \rho}{T^+} \quad (2)$$

where T^+ – sum of positive air temperatures (K) during the same period of n time steps Δt (h), DDF – the degree-day factor in $\text{mm d}^{-1} \text{K}^{-1}$, M_m – measured ablation (m), M – melting (m w.e.), ρ – density (kg m^{-3}). Melting is assumed to be zero when the air temperature is $\leq 0^\circ\text{C}$. The measurement uncertainty of the quantity of melted snow/ice (DM) during time n and the measurement uncertainty of the day-degree factor (DDDF) were determined by the logarithmic derivative method.

Energy balance model. — The energy balance of the glacier surface consists of the following components, following Jania (1993) and Hock (1998):

$$S \pm L \pm Q_h \pm Q_e \pm Q_r + Q_m = 0 \quad (3)$$

where Q_m – the energy available for melting, S – shortwave radiation, L – longwave radiation, Q_h – sensible heat transfer, Q_e – latent heat transfer and Q_r – energy supplied by rain.

Because the temperature at the start of the ablation season stabilizes very rapidly and the melting temperature is maintained throughout the snow cover, the modelling of the energy balance takes no account of the energy flux conducted through the snow cover. From the start of measurements, the temperature at the point of contact between the snow cover and the glacier was 0°C . The temperature within the snow cover oscillated between 0°C and -1°C . With the onset of ablation, the temperature of the entire thickness of the snow cover reached 0°C during one day. Despite subsequent falls of temperature below zero, no changes in the snow cover temperature were recorded. The temperature distribution in the snow cover on Hansbreen in 2010 behaved analogously (Laska 2016). All the measurement and modelling uncertainties were calculated using the total differential or the logarithmic derivative method.

Downwelling shortwave radiation. — The total radiation model was constructed using the Spatial Analyst tool (Area and Point Solar Radiation) in ArcGIS. This software enables spatial and point mapping of total solar radiation, taking into account weather conditions, latitude, altitude above sea level, inclination and exposure, daily and seasonal changes in the solar angle and the effects of shadows thrown by the surrounding topography. In calculations of the total radiation, the ArcGis program does not take into account radiation reflected from orographic barriers. The model of total radiation (S_{dn}) is given by:

$$S_{dn} = S_{dir} + S_{diff} \quad (4)$$

where S_{dir} – direct shortwave radiation, S_{diff} – diffuse shortwave radiation.

To calculate radiation values, the lines of the horizon and shadows were determined for every pixel. In the case of the model used for Werenskioldbreen,

based on DEM generated from the SPOT image obtained on 1 September 2008 (Ignatiuk *et al.* 2015), the *viewshed* was calculated for 64 directions, the values between the directions being interpolated. For calculating the direct radiation, the program creates a *sunmap* for every pixel, that is, the Sun's apparent movement across the sky with the *viewshed* accounted for. The resolution of the map depends on the time interval. The present model used a step of 0.5 h. The scattered radiation is determined using a *skymap* divided into sectors based on the zenithal angle and the Sun's azimuth. A 64x64 grid was used for modelling Werenskioldbreen.

To calibrate the spatial distribution of the total radiation, the latter was determined for a flat surface for a pixel with the position of AWS2 measuring the components of the radiation balance. The model assumed an atmospheric transmissivity equal to 0.7 for the conditions prevailing during the ablation period on the glaciers (Meltofte *et al.* 2008). Based on the total radiation model for a flat surface (S_{modelled}) and the measured total radiation (S_{measured}), the calibration coefficient F was calculated from:

$$F = \frac{S_{\text{measured}}}{S_{\text{modelled}}} \quad (5)$$

where F was the coefficient parameterizing the total radiation model for the surface of Werenskioldbreen. The total radiation sums for the glacier were generated with a 24 h step and a time interval of 0.5 h.

Upwelling shortwave radiation. — The total shortwave radiation is reflected or absorbed by the Earth's surface. The parameter defining the ability of a surface to reflect radiation is the albedo. The value of the reflected radiation (S_{up}) was calculated using the following equation:

$$S_{\text{up}} = \alpha S_{\text{dn}} \quad (6)$$

where S_{dn} – total radiation (scattered and incident), α – albedo.

Albedo. — In order to model the spatial variability of the albedo, the applied method takes account of the sum of positive degree-days (PDD) and the time that has elapsed since the last fall of snow, as proposed by Braithwaite (1995) and further developed by Plüss (1997):

for $T_a \leq 0^\circ\text{C}$

$$\alpha_{T_a \leq 0} = \alpha_{\text{min}} + a_1 \exp(a_2 n_d) \quad (7)$$

for $T_a > 0^\circ\text{C}$

$$\alpha_{T_a > 0} = \alpha_{\text{min}} + a_3 T^{+a_4} \quad (8)$$

where T_a – air temperature, α_{min} – minimum albedo, n_d – number of days since the last snowfall, T^+ – sum of PDD, a_1 to a_4 – empirically determined coefficients

for snow $a_1 = 0.6$, $a_2 = -0.013$, $a_3 = 0.6$, $a_4 = -0.08$, and for ice $a_1 = 0.31$, $a_2 = -0.05$, $a_3 = 0.08$, $a_4 = -0.09$.

This method was further developed by determining separate constants for the snow cover and ice cover. The coefficients a_1 to a_4 were determined on the basis of the albedo measured on the glacier during the 2011 ablation season. The minimum albedo was assumed to be 0.3 for ice and 0.35 for snow.

Downwelling longwave radiation. — The downwelling radiation of the atmosphere was calculated from the following equation:

$$L_{dn} = \varepsilon_a \sigma T_a^4 \quad (9)$$

where L_{dn} – downwelling longwave radiation, ε_a – clear-sky emittance, T_a – air temperature.

The emissivity of the atmosphere for cloudy days was taken to be 0.9 (Plüss 1997). For cloudless days (coefficient F determined for the ratio $S_{\text{measured}}/S_{\text{modelled}} > 0.8$), the formula of Konzelmann *et al.* (1995) including the air temperature (T) and the atmospheric vapour pressure (e) was applied:

$$\varepsilon_a(e, T) = 0.23 + b \left(\frac{e}{T_a} \right)^{\frac{1}{m}} \quad (10)$$

where $m = 7$, $b = 0.635$ tuning parameters determined empirically on the basis of radiation measurements on Werenskioldbreen, e – vapour pressure.

Upwelling longwave radiation. — The Earth's surface radiation is described by the Stefan-Boltzmann Law Eq. (Plüss 1997) which, when the emissivity is taken into account, has the following form:

$$L_{up} = \varepsilon \sigma T_z^4 \quad (11)$$

where L_{up} – upwelling longwave radiation, σ – Stephan-Boltzmann constant, $\sigma = 5.67 \cdot 10^{-8} \text{ W m}^{-2}\text{K}^{-4}$, ε – emissivity, T_z – surface temperature.

For a surface at the melting temperature, longwave emission is naturally limited to 27 MJ m^{-2} per 24 h. The total longwave radiation of the Earth, calculated in this way (3375 MJ m^{-2}) for the ablation period, diverges very considerably from the measured value (3497 MJ m^{-2}). This implies that the surface temperature of the snow/ice must be higher than 0°C . This can be explained by the presence of a thin layer of ablation water on the glacier surface, the temperature of which can rise to above the melting point. In order to take account of this process and to map the values of the surface longwave radiation more accurately, the formula taking the air temperature and the atmospheric radiation has been modified:

$$L_{up} = \varepsilon_a \sigma \left(T_a + T_0 - \frac{T_a + T_0}{T_0} \right) + (1 - \varepsilon_a) L_{dn} \quad (12)$$

where L_{up} – surface radiation, ε_a – clear-sky emissivity (0.99), T_a – air temperature ($^{\circ}\text{C}$), T_0 – absolute zero (-273°C).

Turbulent fluxes. — The fluxes of latent and sensible heat were determined by the aerodynamic method, which is based on the logarithmic distribution of the wind speed (assuming that $z \gg z_0$):

$$u(z) = \frac{u_*}{\kappa} \ln \frac{z}{z_0} \quad (13)$$

where $u(z)$ – wind speed at height z above the ground, u_* – friction velocity (m s^{-1}), κ – von Karman constant ($= 0.40$), z_0 – wind roughness height.

Based on equation (13) the friction velocity (u_*) was calculated for the period 1 May – 10 October 2011. Because of the constant lowering of the glacier surface, the heights of the wind speed sensors changed with time. This disrupted the pattern of the friction velocity. In consequence, a coefficient was determined to correct the friction velocity based on the initial positions of the sensors and their temporal variability.

The gradient method was used to determine the heat fluxes, as described by the equation after Hock (1998) and Andreas *et al.* (2002, 2005a, 2005b):

$$Q_h = \rho_p c_p C u_z (T_z - T_s) \quad (14)$$

where ρ_p – density of air (kg m^{-3}), c_p – specific heat capacity of air ($\text{J kg}^{-1} \text{deg}^{-1}$), u_z – wind speed at height z above the ground, T_s – surface temperature ($^{\circ}\text{C}$), T_z – air temperature at height z above the ground, C – exchange coefficient.

The equation for the latent heat, under melting conditions and applying the vapour pressure of water as a variable instead of the humidity, takes the form (Hock 1998; Singh and Singh 2001):

$$Q_e = 0.623 L_v \frac{\rho_0}{P_0} C u_z (e_z - e_0) \quad (15)$$

where L_v – latent heat of evaporation (J kg^{-1}), P_0 – standard atmospheric pressure (1013 hPa), ρ_0 – air density at pressure P_0 (1.29 kg m^{-2}), e_0 – vapour pressure of a melting surface (611 Pa), e_z – vapour pressure at height z .

The vapour pressure of water (e_z) was calculated on the basis of two equations (Marsz 2002):

$$e_z = E H \quad (16)$$

$$E = 3 \cdot 10^{-6} T^4 + 0.013 T^2 + 0.415 T + 6.171 \quad (17)$$

where E – maximum vapour pressure of water at a given temperature, H – humidity expressed as a decimal number, T – air temperature.

Simplified formulas are used in this paper in which only the roughness parameter is taken into consideration in the heat exchange coefficient (Singh and Singh 2001):

$$C = \frac{k^2}{[\ln(\frac{z}{z_0})]^2} \quad (18)$$

for the snow cover, coefficient C was calculated as $C = 0.0018$ and the literature value of $C = 0.0020$ was taken for the ice surface (Plüss 1997).

Energy supplied by rain. — For the conditions under which the snow cover melts, the amount of heat was calculated from the following formula (Hock 1998):

$$Q_r = \rho_w c_w R(T_r - T_s) \quad (19)$$

where ρ_w – density of water (kg m^{-3}), c_w – specific heat of water ($4.2 \text{ kJ kg}^{-1} \text{ K}^{-1}$), R – precipitation (mm), T_s – surface temperature (0°C), T_r – rain temperature (0°C). The model utilized the amount of rainfall measured at the Polish Polar Station in Hornsund (PPS Hornsund) meteorological observatory, which is registered in the WMO (World Meteorological Organisation) as number 01003 (Wawrzyniak and Osuch 2020).

Energy for melting. — In the period when the snow cover is absorbing energy, there comes a moment when 0°C is reached, at which temperature all excesses of energy are used up for melting. The energy for melting was calculated from the formula:

$$Q_m = M \rho_w L_f \beta \quad (20)$$

where Q_m – energy for melting ($\text{kJ m}^{-2} \text{ day}^{-1}$), M – melt rates (m day^{-1}), L_f – latent heat of fusion (333.6 J g^{-1}), ρ_w – density of water (kg m^{-3}), β – thermal quality of snow (0.97).

This equation can be transformed in order to determine the 24 h ablation. After taking above equations into consideration, the following one defines the volume of ablation water given by the energy balance model :

$$M = \frac{Q_R \pm Q_h \pm Q_e}{Q_m} \quad (21)$$

$$M = \frac{S_{dn} + (S_{dn} \alpha) + L_{dn} + L_{up} \pm \rho_p c_p C u_z (T_z - T_s) \pm 0.623 L_v \frac{\rho_0}{P_0} C u_z (e_z - e_0)}{\rho_w L_f \beta} \quad (22)$$

Equation 22 was used to model the quantity of ablation water formed on Werenskioldbreen in the 2011 summer season. The model was validated by comparing the ablation modelled with that measured with an SR50 sensor at the AWS2.

Results

Meteorological and glaciological conditions in 2011. — The ablation season in 2011 began on 30 May at station AWS1 and on 12 June at AWS2 (Fig. 2). Towards the end of the ablation season, on 3 October, the mean daily air temperatures were below zero at both stations. In June at the lower station, there were 3 days with a mean negative temperature, whereas at the upper station following the onset of ablation in June there was only one such day. In July, no days were recorded with a mean air temperature below 0°C. In August, there were 0 and 2 days with a negative 24 h air temperature at the lower and upper stations respectively, while in September there were 3 such days at each station.

On the basis of the accumulated data, the temperature gradient in the 2011 ablation season was calculated at 0.53°C per 100 m. The vertical air temperature gradient in the surface layer of the atmosphere was also analysed. At station WRN2 the temperature gradient for the 2011 ablation season was -0.30°C per 1.5 m, while at WRN1 it was -0.34°C per 1.5 m.

The mean annual air temperatures at AWS1 and AWS2 were 1.5°C and 2.1°C lower, respectively, than those measured at the PPS Hornsund. During the ablation season, June and September were the months when the mean temperature at PPS Hornsund was higher than the long-term value (Table 1).

Table 1.

Mean monthly air temperatures on Werenskioldbreen (AWS1, AWS2) and in the PPS Hornsund from May 2010 to December 2011, compared with the long-term values from 1979–2011 in Hornsund (Wawrzyniak and Osuch 2020).

Month	Air temperature (°C)			
	Hornsund	AWS1	AWS2	Hornsund 1979–2018
January	-12.5	-13.5	-14.0	-9.7
February	-9.4	-9.4	-10.4	-9.8
March	-9.8	-10.9	-11.8	-10.2
April	-3.7	-6.2	-7.1	-8.1
May	-1.6	-2.9	-4.1	-2.5
June	3.2	1.6	0.8	2.5
July	3.9	2.8	2.2	4.6
August	4.2	3.4	3.2	4.2
September	4.1	3.1	2.5	1.8
October	-0.9	-3.0	-3.6	-2.7
November	-3.8	-5.8	-6.3	-5.7
December	-4.6	-7.9	-7.3	-8.6
Average	-2.6	-4.1	-4.6	-3.7

The mean humidity for the analysed period in the PPS Hornsund was 84%, but 90% and 92% for AWS2, at respective heights of 2 m and 0.5 m. Daily mean fluctuation of the humidity at a height of 0.5 m was lower (4.5%) than at 2 m (7.0%) and at the PPS Hornsund (8.1%).

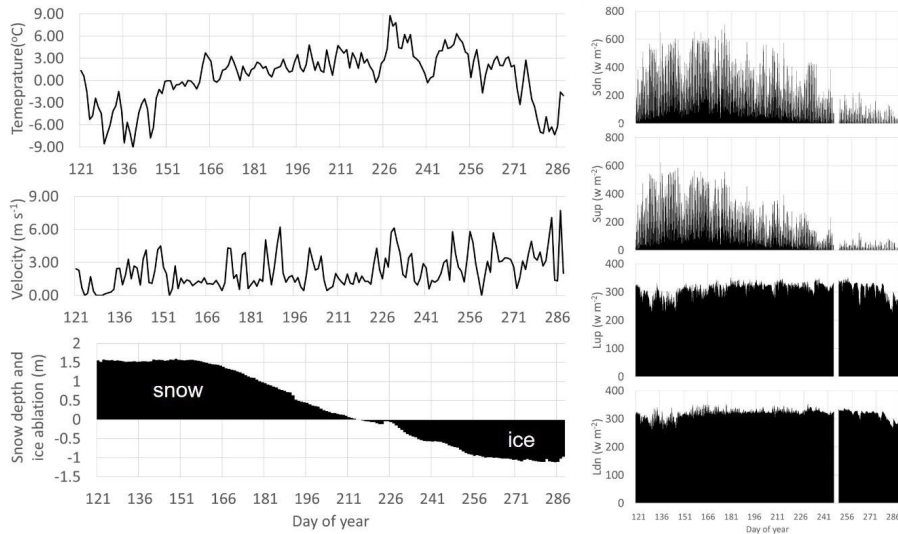


Fig. 2. Time series of meteorological variables in the ablation season 2011 on Werenskioldbreen (AWS2), including daily average air temperature, daily wind speed, daily ablation, hourly shortwave downwelling (Sdn) and upwelling (Sup) radiation and hourly longwave downwelling (Ldn) and upwelling (Lup) radiation.

Knowledge of the wind speed distribution over the glacier surface is a key aspect when modelling of the energy balance. The distribution of the topographic index (DEM-based) of wind exposure can be used to better calculate the wind speed distribution. Unfortunately, in the present case, the wind direction was not measured due to the lack of space for appropriate sensors at the AWS. The mean 24 h wind speed at a height of 2 m at AWS2 is greater than that at the PPS Hornsund. The mean vertical wind speed gradient between the sensors on the glacier was 1.46 m s^{-1} for the entire measurement period and 1.07 m s^{-1} for the ablation period. For the latter period, the gradient rose linearly with increasing wind speed. The maximum 24 h gradients between 0.5 and 2 m were recorded on 9 May 2011 (9.97 m s^{-1}) and on 7 April 2011 (8.97 m s^{-1}). During the ablation period, such maximum gradients were recorded on 9–10 July (5.61 ; 542 m s^{-1}) and on 13–14 September (5.88 ; 5.68 m s^{-1}).

The annual radiation balance at AWS2 was 112.2 MJ m^{-2} . For 9 months of the year (January–May, October–December), the radiation balance was negative. This was due to the way in which the radiation balance was affected by longwave radiation during the polar night. The negative balance in March and April resulted from the minimal influx of shortwave radiation, as the Sun was still low

over the horizon. In May, even though the total incident shortwave radiation (567.4 MJ m^{-2}) was almost as great as in June (599.0 MJ m^{-2}), the radiation balance was still negative because of the high albedo. In June, the incident radiation reached a peak (Table 2), because the Sun then reaches its greatest height above the horizon, but it is in July and August that the greatest amount of shortwave radiation reaches the glacier surface. This is because of the constant decrease in the albedo in the summer months. The mean monthly albedo varied from 0.42 to 0.97 (Table 2).

Table 2.

Monthly sums of incident and reflected shortwave radiation and emitted longwave radiation in 2011 on Werenskioldbreen (AWS2). S_{dn} – downwelling shortwave radiation, S_{up} – upwelling shortwave radiation, L_{dn} – downwelling longwave radiation, L_{up} – upwelling longwave radiation, Net S – net balance of shortwave radiation, Net L – net balance of longwave radiation, Net radiation – net balance of shortwave radiation and longwave radiation.

Month	S_{dn}	S_{up}	L_{up}	L_{dn}	Net S	Net L	Net radiation	Albedo
	(MJ m ⁻²)							
January	0.0	0.0	672.7	642.9	0.0	-29.8	-29.8	
February	4.8	3.5	642.8	609.0	-1.3	-33.8	-35.1	
March	112.3	99.5	693.2	661.2	-12.8	-32.0	-44.8	
April ¹	123.5	123.0	388.9	378.6	-0.5	-10.3	-10.8	
May	567.4	585.6	804.3	760.4	18.2	-43.9	-25.8	0.97
June	599.0	699.9	839.4	797.8	100.9	-41.6	59.3	0.86
July	350.4	483.4	871.4	863.1	133.0	-8.2	124.8	0.72
August	189.0	320.7	871.5	854.8	131.8	-16.7	115.1	0.59
September ²	31.0	73.4	723.7	715.6	42.4	-8.2	34.3	0.42
October	14.8	17.1	791.0	759.2	2.3	-31.8	-29.5	0.86
November	0.0	0.0	733.6	715.3	0.0	-18.3	-18.3	
December	0.0	0.0	742.1	714.8	0.0	-27.2	-27.2	
SUM	1992.1	2406.1	8774.5	8472.7	414.0	-301.8	112.2	
MEAN	166.0	200.5	731.2	706.1	34.5	-25.1	9.3	0.7

¹ no measurements for 14 days; ² no measurements for 4 days

The glacier-wide surface mass balance in 2011 was -38.10 m^3 , while for the winter and summer it was 13.3 m^3 and -51.4 m^3 , respectively. The winter point balance varied from 0.72 to 1.97 m (Table 3), its linear pattern being related to altitude above sea level. In the winter season of 2011, snow did not accumulate directly on the glacier front, which is steep. The summer point balance indicates that the highest ablation occurred in the lowest zones of the glacier (-2.60 m w.e.).

Table 3.

Characteristics of snow cover, ablation stakes (WRN1 to WRN9) and elements of the glacier mass balance in 2011.

	Ablation stake height a.s.l. (m)	Snow cover depth	Average bulk snow density (kg m^{-3})	Winter point mass-balance (m w.e.)	Summer point mass-balance (m w.e.)	Annual point mass-balance (m w.e.)
WRN1	515	1.97	357	0.70	-1.36	-0.66
WRN2	384	1.55	379	0.59	-1.68	-1.09
WRN3	471	1.85	421	0.78	-1.30	-0.52
WRN4	392	1.36	423	0.58	-1.25	-0.67
WRN5	308	1.74	408	0.71	-1.66	-0.95
WRN6	188	0.72	408	0.29	-2.61	-2.31
WRN7	199	1.55	460	0.71	-2.14	-1.43
WRN8	277	1.31	414	0.54	-2.02	-1.48
WRN9	120	0	0	0.00	-2.60	-2.60

The annual point balance confirms the field observations of no accumulation on Werenskioldbreen (Table 3). In 2011, the equilibrium line altitude was above the glacier surface.

Temperature index model. — Two temperature models were carried out for 2011. They were based on determining the degree-day factor (DDF) for snow and ice at both stations AWS1 and AWS2 (Table 4). Air temperature data from the two stations were used in the modelling. With the SR50 sensor it was possible to define precisely the instant at AWS2 when the snow cover finally disappeared, which meant that the model was better adapted to the real measurements of ablation (Fig. 3).

The best temperature model for 2011 from AWS2 was compared with the ablation measured with the SR50 sensor at the weather station on Werenskioldbreen (Fig. 3). The model obtained during the snow cover ablation period has a tendency to underestimate ablation but to overestimate this during the ice ablation period. The modelled ablation for the entire glacier was -44.86 m^3 , compared with -51.4 m^3 calculated from measurements at the ablation stakes (Fig. 4).

Energy balance model. — The sum of radiation measured from 1 June until 3 October was 1580 MJ m^{-2} , compared with the modelled total of 1520 MJ m^{-2} . The discrepancy between the modelled and real values could be due to the fact that the model did not take reflected radiation into account, which in a landscape with snow-covered slopes plays an important part in the sum of total radiation. The sum of the measured reflected radiation for the entire 2011 ablation season was 1171 MJ m^{-2} , compared with 1159 MJ m^{-2} for the modelled sum of reflected

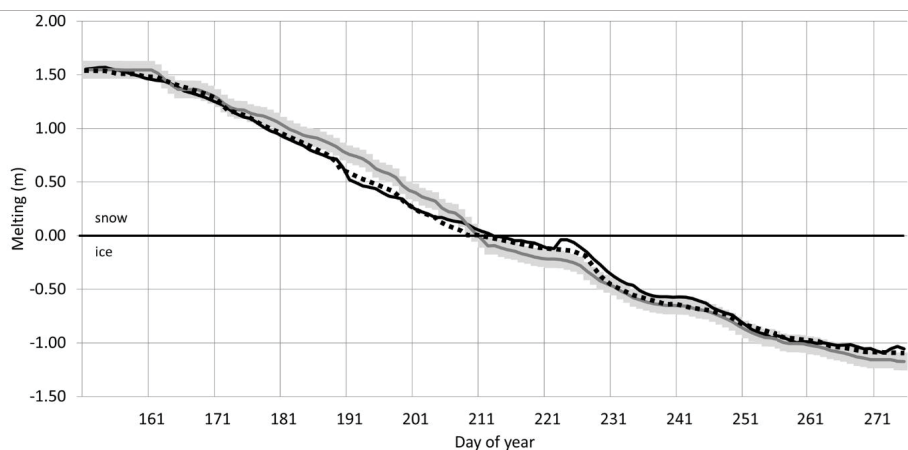


Fig. 3. The measured ablation on AWS2 (black line) with the ablation calculated from the temperature-index model (grey line) and energy balance model (dotted line). Bars indicate uncertainties.

Table 4.

Calculated positive degree-day factors (DDF) for ice and snow on Werenskioldbreen in 2010 and 2011. T+ – sum of positive air temperatures.

	AWS2					AWS2 1				
	T ⁺	DDF snow	Δ DDF	DDF ice	Δ DDF	T ⁺	DDF snow	Δ DDF	DDF ice	Δ DDF
2011	179.61	6.24	0.22	5.31	0.13	244.4	9.9	0.36	5.5	0.13

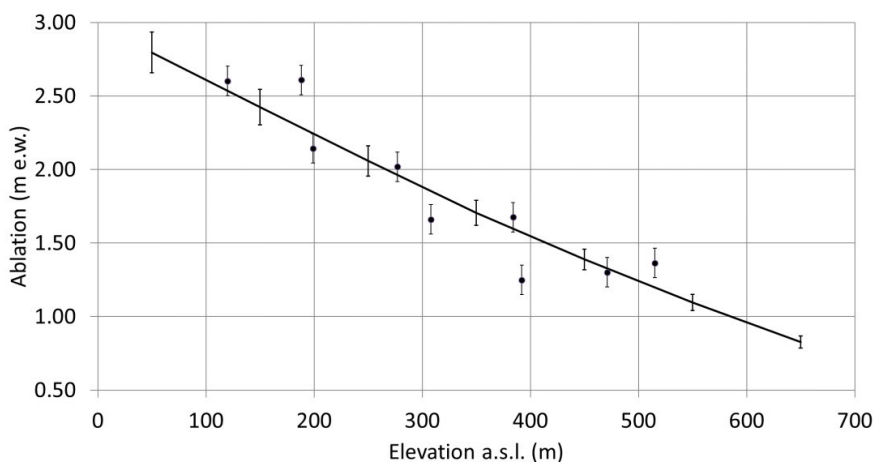


Fig. 4. The measured ablation on mass-balance stakes (black dots) with the ablation calculated from the temperature-index model (black line). Bars indicate uncertainties.

radiation. The sum of atmospheric radiation measured for the period 1 June to 3 October 2011 was 3420 MJ m^{-2} , whereas the modelled sum was 3415 MJ m^{-2} .

The computed sum of the Earth's longwave radiation (3375 MJ m^{-2}) for the ablation period differs from the measured value (3497 MJ m^{-2}) because the temperature of the snow/ice surface can be higher than 0°C . This is due to the presence of a thin layer of ablation water on the glacier surface, which may reach a temperature above the melting point. But in spite of these oscillations, the dependence between the models is $R^2 = 0.68$ (adjusted $R^2 = 0.64$), and the sum of radiation measured for the whole season (3497 MJ m^{-2}) is close to the modelled sum (3488 MJ m^{-2}).

The modelled albedo, based on snow cover data acquired from the SR50 sensor, was compared with the measurement data at AWS2 (Fig. 5).

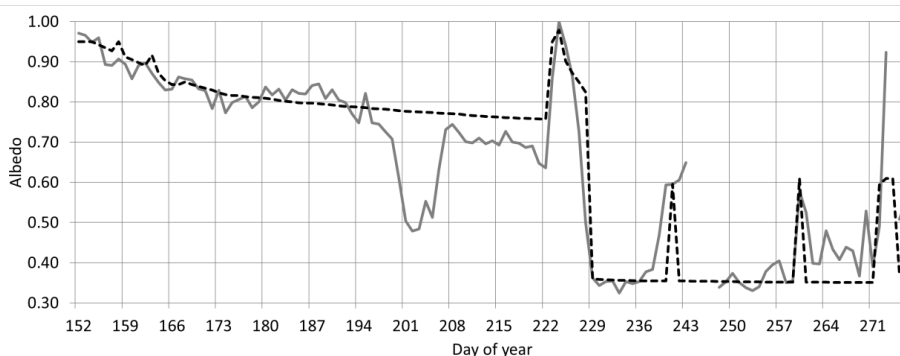


Fig. 5. Albedo measured on AWS2 (grey line) and modelled (dashed line) during the 2011 ablation season on Werenskioldbreen.

Here, we see a drop in the albedo together with the ageing of the snow cover and its contamination, mainly by dusts blown in from the surrounding slopes. The humidity of snow, affected as it is by the weather, also has a substantial influence on the albedo. The coefficient of determination R^2 between the measured and modelled albedo is equal to 0.812. So long as snow cover is present, the model gives a good representation of the albedo's variability. But there was a considerable discrepancy between the modelled and measured values between 19 and 27 July. This was due to the lower level of reflected radiation during this period. Jonsell *et al.* (2003) stated that when the sky is cloudless, the daily fluctuations of the albedo can reach a value of 0.3 on a horizontal surface. The pattern of the albedo exhibits distinct periods when the air temperature is below 0°C . The increase in the albedo at such times is probably due to the freezing of the ice surface, condensation of water vapour or snowfall.

The calculated latent heat values are very small in comparison with the other components of the energy balance. The 24 h pattern of latent heat depends on the wind speed and the water vapour pressure gradient. The 24 h minima are associated with higher air temperatures and lower air humidity. The maximum

values in the first half of September result from the overlap of high water vapour pressures and high wind speeds. The 24 h pattern of sensible heat has a much larger amplitude of changes and high levels of energy supplied to the glacier surface. The maximum sensible heat values are associated directly with periods with higher wind speeds. In the spatial distribution, the highest sensible heat values are recorded in the frontal zone of the glacier and decrease with height. This is directly due to the spatial distribution of temperature on the glacier. The latent heat pattern is the converse of that of sensible heat. In the glacier frontal zone, the sums of latent heat are negative and increase with height, becoming positive in the highest parts of the glacier.

During the ablation period, no long spells with below-zero temperatures were recorded, in spite of the energy supplied by rain freezing within the snow cover. It is worth noting, however, that when rain falls at a speed of 1 mm per hour on to a surface with parameters $T_s = -3^\circ\text{C}$, $\rho_s = 240 \text{ kg m}^{-3}$, $d_s = 0.3 \text{ m}$ and $T = 0^\circ\text{C}$, the temperature of the snow cover increases at a rate of 0.6°C per h . Under such conditions the temperature of the snow will rise to 0°C within 5 hours (Singh and Singh 2001).

The spatial model of the energy supplied by rain utilizes the calculated temperature gradient and also a vertical precipitation gradient of 10% per 100 m (Migała personal communication). The calculated overall amount of energy supplied by rain in the summer of 2011 was so low compared with the other fluxes that it was not included in the balance ($1.56\text{--}4.67 \text{ kJ m}^{-2}$).

The pattern of ablation, measured and modelled on the basis of the energy balance, shows a very good correlation – $R^2 = 0.998$. The model shows a two-day delay in calculating the eventual disappearance of the snow cover, but this does not have a negative effect on the overall value of ablation. The point ablation estimated on the basis of the energy balance model is 1.63 m w.e. Point ablation measured with an SR50 sensor was 1.60 m w.e. The modelled pattern of ablation gives a very good reflection of this process, which means that it can be used in spatial modelling (Fig. 3).

The initial conditions of the model, regarding the snow cover distribution, were defined on the basis of determined dependences of this distribution on altitude. The model utilizes the spatial distribution of shortwave radiation, which takes account of the spatial variability of the albedo and the spatial distribution of the longwave radiation balance, which in turn takes the spatial distribution of air temperature on the glacier into consideration. Calculated gradients of air temperature, humidity and wind speed were used for modelling the spatial differentiation of turbulent energy exchange fluxes. The spatial distribution of air temperature was used for calculating the sensible heat and the water vapour pressure for latent heat.

The resulting spatial model of ablation confirms the lack of accumulation on the glacier in 2011. The greatest ablation was recorded in the frontal zone of the glacier and diminished with altitude. There are clearly-defined zones on the glacier where

ablation is less because of the topography, *e.g.* the southern edge of the glacier at the foot of Angellfjellet. The highest-lying parts of the glacier are differentiated with respect to the magnitude of ablation because of the different exposures of the surface. South-facing surfaces are subject to greater ablation than north-facing ones, which are often additionally obscured by mountain ridges.

The altitude zones between 200 and 500 m a.s.l. are where the largest volumes of ablation water are produced (Table 5). This is crucial for the magnitude of the glacier's internal supply. Water percolation zones, mapped by SAR, cover only 5% of the area of the zone between 200 and 300 m a.s.l., but 45% and 95% of the area of the two higher zones.

The quantitative proportions of the various components of the energy balance in particular altitude zones are illustrated in Fig. 6. This shows the increasing participation of the various components of the balance, which reach a maximum between 300 and 400 m a.s.l., where the greatest volumes of meltwater originate. Because of its size, the next higher altitude zone still absorbs large amount of energy. Given ongoing climate warming, this zone is likely to be a major source of ablation waters.

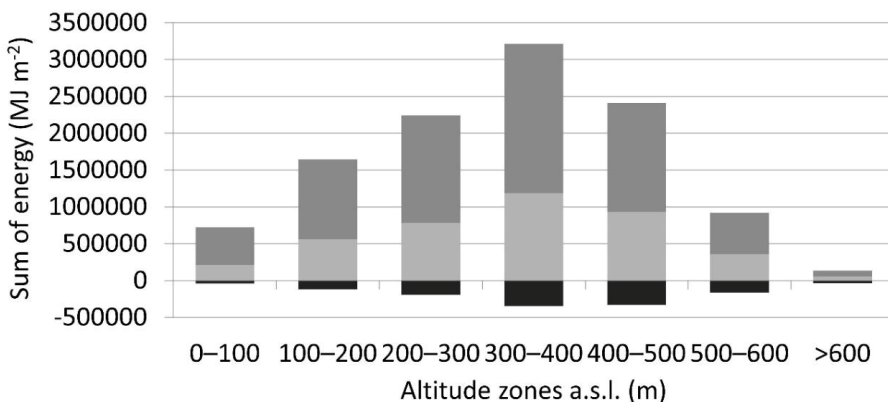


Fig. 6. Main components of the energy balance for altitude zones on Werenskioldbreen during the 2011 ablation season. Sensible heat is marked in light gray, the balance of shortwave radiation in dark gray and balance of longwave radiation in black.

Analysis of proportion of the various components of the energy balance (Fig. 7) shows that the percentage of the shortwave radiation balance decreases with altitude from 65% to 46%. At the same time there is an increase (up to 20%) in the longwave radiation balance. Sensible heat is subject to the smallest fluctuations, increasing in the zones from 0 to 200 m a.s.l., where a constant level is maintained (*ca.* 35%). The values of latent heat on Werenskioldbreen are very low, less than 1%.

In cloudless weather, the energy balance is mediated mainly by shortwave and longwave radiation. The latter may make up as much as 57% of the 24 h energy balance. Such values were recorded at the beginning and end of the

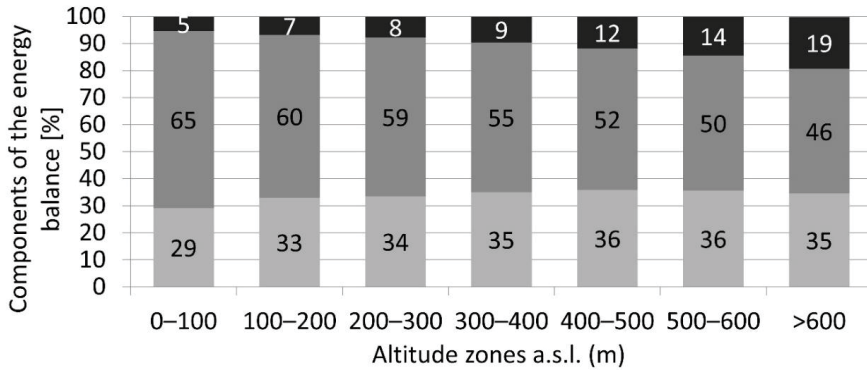


Fig. 7. Main components of the energy balance for altitude zones on Werenskioldbreen during the 2011 ablation season. Sensible heat is marked in light gray, the balance of shortwave radiation in dark gray and balance of longwave radiation in black.

ablation season, when air temperatures were below zero. At other times during the season, longwave radiation contributed no more than 35% to the energy balance. In extreme instances, when air temperatures are high and the sky cloudless, the sensible heat flux may supply 50% of the energy balance, and in conditions of extensive cloudiness as much as 75%. The ablation estimated on the basis of the energy balance model for the whole glacier was -49.6 m^3 (Fig. 8), compared with -51.4 m^3 calculated on the basis of measurements from ablation stakes.

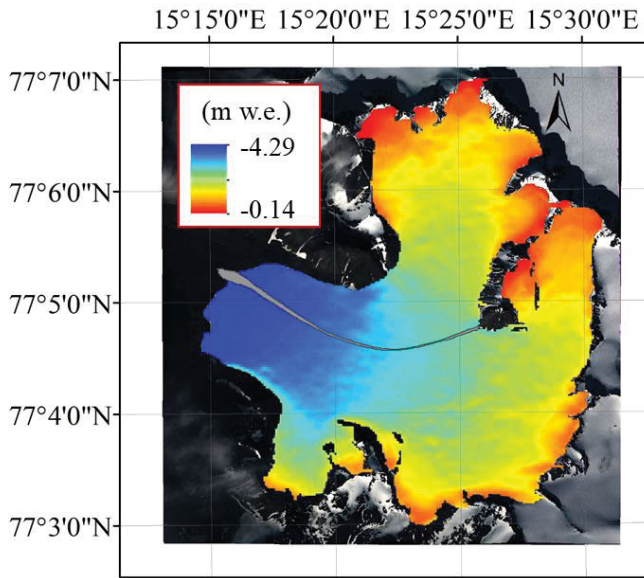


Fig. 8. Spatial distribution of ablation on Werenskioldbreen during the ablation season of 2011 on the basis of the energy balance model (background: GeoEye-1 VHSR image acquired on 10 August 2010).

Table 5.

Comparison of ablation values for given altitude zones based on the mass balance, the temperature-index model and the energy balance model for Werenskioldbreen in 2011.

Altitude zone (m a.s.l.)	Glacier-wide mass balance (10^6 m^3)	Temperature-index model (10^6 m^3)	Energy balance model (10^6 m^3)
0–100	2.55 ± 0.13	2.27 ± 0.04	3.36 ± 0.17
100–200	6.65 ± 0.33	6.02 ± 0.33	7.51 ± 0.38
200–300	9.54 ± 0.48	8.39 ± 0.77	10.10 ± 0.51
300–400	14.92 ± 0.75	12.86 ± 2.25	14.14 ± 0.71
400–500	12.17 ± 0.61	10.43 ± 1.89	10.26 ± 0.51
500–600	4.80 ± 0.24	4.18 ± 0.43	3.74 ± 0.19
>600	0.79 ± 0.04	0.71 ± 0.02	0.50 ± 0.03
Total	51.42 ± 2.57	44.86 ± 5.73	49.61 ± 2.48

Discussion

The mass balance in 2011 was compared with data from (WGMS 2021) and Ignatiuk *et al.* 2022). The mean winter balance in 2011 was clearly higher than in 1994 and 1999–2000. The summer balance of Werenskioldbreen in 2009–2011 was much higher than in 1999–2000, despite the mean temperature for the summer months measured at the PPS Hornsund, being practically the same in both periods (3.3°C for 1999–2000 and 3.4°C for 2009–2011) (Wawrzyniak and Osuch 2020). The summer balance in 1994 was far less than that measured in other years, among other because of the very cool summer with the mean temperature in the summer months at 2.3°C . The summer balance values for Werenskioldbreen were higher than those recorded on the Hans Glacier ($R=0.72$). In addition, the point ablation measurements from 1956–1962 and 1969–1974 (Kosiba 1960; Baranowski 1977; WGMS 2021), equal to 1.35 m as compared with 2.35 m in 1998–2001 and 2.64 m in 2009–2011, indicate that ablation on Werenskioldbreen was increasing. Nevertheless, at the scale of the last decade, no statistically significant trends have been observed, whether in the winter, summer or net balance (Ignatiuk *et al.* 2022).

The temperature-index ablation model is based on the air temperature gradient determined for Werenskioldbreen. The air temperature gradient calculated for the 2011 ablation season (0.53°C per 100 m) was similar to that determined for 1970 (0.55°C per 100 m) (Baranowski 1975) and for 1979 (0.52°C per 100 m) (Pereyma *et al.* 1974). In spite of on-going climate warming in the Arctic (Hanssen-Bauer *et al.* 2019), the air temperature gradient on Werenskioldbreen has not changed. For the periods analysed, this parameter is smaller than those recorded on other glaciers, which lie within the range from 0.6 to 1.0°C per 100 m (Bruland and Hagen 2002).

Table 6.

Comparison of degree-day factors (DDF) given in the literature with those measured on Werenskioldbreen.

Location	DDF snow	DDF ice	Latitude	Altitude (m a.s.l.)	Reference
Alfotbreen, Norway	4.5	6	61°45'N	850–1400	Laumann and Reeh (1993) ¹
Hellstugubreen, Norway	3.5	5.5	61°34'N	1450–2200	
Nigardsbreen, Norway	4	5.5	61°41'N	300–2000	
Storglaciären, Sweden	4.4	6.4			Jóhannesson <i>et al.</i> (1995) ¹
	3.2		67°55'N	1550	Hock (1998)
		6		1370	
		6.4		1370	
		5.4		1250	
Vestfona, Spitsbergen		13.8	~80°N	310–410	Schytt (1964) ¹
Satujökull, Iceland	5.6	7.7	~65°N	800–1800	Jóhannesson <i>et al.</i> (1995) ¹
South Glacier (Alaska)	5.4	14	61°N	1970–2960	Wheler (2004)
North Glacier (Alaska)	1.6	11	61°N	1890–3100	
Werenskioldbreen	5,1	7,1	77°N	40–700	This paper

¹ after Hock (2003)

The DDF calculated for 2011 remains within the intervals given by Hock (2003) and Zhang (2000) (Table 6). Even though temperature models work well in the long term, their accuracy is considered to decrease with increasing temporal resolution. There are also gaps in these models when they relate to terrain with a varied topography, since they take no account of either the *viewshed* or the inclination and exposure of slopes (Hock 2003).

The calculated roughness parameter (z_0) corresponds to the literature values measured on glaciers (Table 7). For a surface devoid of snow cover, the value of the heat exchange coefficient (C) was taken to be $2.0 \cdot 10^{-3}$ m. The calculated value of C for an ice surface ($C=1.8 \cdot 10^{-3}$ m) lies within the range ($0.12\text{--}2.2 \cdot 10^{-3}$ m) determined for glaciers on the basis of field measurements (Paterson 1994; Plüss 1997; Klok and Oerlemans 2002).

The temperature-index and energy balance models were validated by comparison with ablation measured by the SR-50 sensor at AWS2. Ablation near that station was well reflected by both models. With the onset of intense ablation in mid-June, the temperature model clearly underestimated the

Table 7.

Roughness parameters z_0 of ice and snow surfaces obtained by different authors modified after Singh and Singh (2001).

Source reference	Roughness parameter z_0 (cm)	
	snow	ice
Grainger and Lister (1966)	–	0.04
Sevruk (1982)	0.5	–
Ambach (1986)	0.01	0.2
Harding (1986)	0.02 – 0.38	–
Braithwaite (1995)	0.01	0.2
This study	0.01	–

magnitude of ablation, but once the ice had begun to melt, the modelled values of ablation were now overestimated. The pattern of the energy balance model exhibited clearly fewer fluctuations and a smaller deviation from the measured ablation. There was a very close dependence ($R=0.99$) between the pattern of measured ablation and that calculated from the two models. Nonetheless, the value calculated from the temperature model (1.71 m w.e.) was much higher than the measured value (1.60 m w.e.). The ablation calculated using the energy balance model was 1.63 m w.e. The temperature-index model underestimates ablation in all zones, in particular between 300 and 500 m a.s.l. (Table 5). This is due to underestimation of the snow ablation, which is visible when compared to the SR50 (Fig. 3). The energy balance model tends to overestimate the ablation in the lowest zones of the glacier (0–200 m a.s.l.). This can be influenced by the occurrence of temperature inversions, which may result in lower observed ablation in the frontal area of Werenskioldbreen.

The percentage participation of the components of the balance were calculated on the basis of the energy balance model (Table 8). The energy balance was shaped primarily by the radiation balance and sensible heat. The contribution of the latent heat flux on Werenskioldbreen was minimal, less than 1%. A high contribution of sensible heat to ablation is given by Hodson *et al.* (2005) and Hulth *et al.* (2008) for glaciers on Spitsbergen and Jan Mayen (Table 8). On Werenskioldbreen, the contribution of sensible heat was greater. However, on the basis of one year's measurements, it is very difficult to judge whether this is characteristic of this particular glacier or merely specific to 2011. Migala *et al.* (2006) calculated the contributions of the various components of the energy balance for the Hans Glacier, which lies immediately adjacent to Werenskioldbreen. The proportion of sensible heat for the Hans Glacier in 2004 was 18.2% (Table 8), which suggests that the year 2011 was an exceptional one in the Hornsund region or that permanent changes have occurred in the energy balance of the glaciers in southern Spitsbergen.

Table 8.

Percentage distribution of energy balance components of Northern Hemisphere glaciers.

Glacier	Radiation balance	Sensible heat	Latent heat	Reference
Hans Glacier (Spitsbergen)	76.1	18.2	5.7	Migala <i>et al.</i> (2006)
South Glacier (Canada)	96.1	8.3	-0.6	Wheler (2004)
Storglaciären (Sweden)	66	30	5	Hock (1998)
Storbreen (Norway)	76	17.0	8	Andreassen <i>et al.</i> (2008)
Sørbreen (Jan Mayen)	48.5	33.8	17.6	Hulth <i>et al.</i> (2008)
Midre Lovenbreen (Svalbard)	73.9	18.9	7.2	Hodson <i>et al.</i> (2005)
McCall Glacier (Alaska)	74.4	24.8	4.8	Klok <i>et al.</i> (2005)
Werenskioldbreen (Svalbard)	58	42	<1	This paper

With the ablation values obtained from the model for the various altitudinal zones (Fig. 8 and Table 5), one can calculate the volumes of ablation water formed on the glacier surface. The zone where most of this water was produced is the one between 400 and 500 m a.s.l., 95% of which is a firm area, and also the one between 300 and 400 m a.s.l., where firm covers 45% of the surface. The total runoff of the Breelva (Majchrowska unpublished) in 2011 was $79.6 \cdot 10^6 \text{ m}^3$, a value greater than that obtained with the models. It should be kept in mind that this total runoff includes snow melt and rainfall from the non-glaciated parts of the catchment (35% of this area), the melting of permafrost and laminar flow on the forefield (Stachniak *et al.* 2022).

Conclusions

This paper discusses the modelling of glacier surface ablation by the temperature-index and energy balance models as well as the results of meteorological and glaciological studies on Werenskioldbreen (Svalbard) in 2011. The energy balance model offers a better fit to the field measurements than the temperature-index model. When modelling the energy balance, the model has to be validated and calibrated with meteorological measurements, which provides the relevant gradient and calibration data for modelling the radiation balance. The

energy balance modelling results showed that the radiation balance (58%) and sensible heat (42%) are the main factors influencing surface ablation on the glacier. These models are highly suited for calculating ablation in Svalbard and other areas in the Arctic.

Acknowledgements. — The studies were carried out with the use of research and logistic equipment (monitoring and measuring equipment, sensors, multiple AWS, GNSS receivers, snowmobiles and other supporting equipment) of the Polar Laboratory of the University of Silesia in Katowice. The author thank the employees, doctoral students and students of the University of Silesia in Katowice for their help in the fieldwork. He would also like to thank colleagues from the University of Wrocław for their hospitality at the Stanisław Baranowski Polar Station. Special acknowledgments to Jacek Jania for scientific discussions and support during doctoral studies, when most of the data for this article has been collected. The author would like to acknowledge Peter Senn for the linguistic proofreading and two anonymous reviewers for their constructive reviews.

References

- Ambach W. 1986. Nomographs for the determination of meltwater from snow- and ice surfaces. *Berichte des Wissenschaftlich-Medizinischen Verens in Innsbruck* 73: 7–15.
- Andreas E.L. and DeCosmo J. 2002. The signature of spray in the hexos turbulent heat flux data. *Boundary-Layer Meteorology* 103: 303–333. doi: 10.1023/A:1014564513650
- Andreas E.L., Brunke M.A., Zeng X. and Zhou M. 2005a. An intercomparison of model bulk aerodynamic algorithms used over sea ice with data from the SHEBA experiment. *Journal of Geophysical Research* 111: C09001. doi: 10.1029/2005JC002907
- Andreas E.L., Jordan R.E. and Makshtas A.P. 2005b. Parametrizing turbulent exchange over Sea Ice: The Ice Station Weddell results. *Boundary-Layer Meteorology* 114: 439–460. doi: 10.1007/s10546-004-1414-7
- Andreassen L.M., Van Den Broeke M.R., Giesen R.H. and Oerlemans J. 2008. A 5 year record of surface energy and mass balance from the ablation zone of Storbreen, Norway. *Journal of Glaciology* 54: 45–258. doi: 10.3189/002214308784886199
- Baranowski S. 1975. Glaciological investigations and glaciomorphological observations made in 1970 on Werenskiold Glacier and in its forefield, Glaciological investigations of the Polish Scientific Spitsbergen Expeditions 1970–1974, Vol. 1. *Acta Universitatis Wratislaviensis* 251: 69–94.
- Baranowski S. 1977. The subpolar glaciers of Spitsbergen seen against the climate of this region. *Acta Universitatis Wratislaviensis* 410: 94 pp.
- Baranowski S. 1982. Naled ice in front of some Spitsbergen glaciers. *Journal of Glaciology* 28: 211–214. doi: 10.3189/S0022143000011928
- Błaszczuk M., Jania J. A. and Kolondra L. 2013. Fluctuations of tidewater glaciers in Hornsund Fjord (Southern Svalbard) since the beginning of the 20th century. *Polish Polar Research* 34: 327–352. doi: 10.2478/popore-2013-0024
- Błaszczuk M., Jania J. A., Cieplý M., Grabiec M., Ignatiuk D., Kolondra L., Kruss A., Luks B., Moskalik M., Pastusiak T., Strzelewicz A., Walczowski W. and Wawrzyniak T. 2021. Factors controlling terminus position of Hansbreen, a tidewater glacier in Svalbard. *JGR Earth Surface* 126: 327–352. doi: 1029/2020JF005763

- Braithwaite R. J. 1995. Positive degree-day factors for ablation on the Greenland ice sheet studied by energy-balance modelling. *Journal of Glaciology* 41: 153–160. doi: 10.1017/S0022143000017846
- Braithwaite R. J. and Olesen O. B. 1989. Calculation of glacier ablation from air temperature, West Greenland. In: Oerlemans J. (ed.) *Glacier fluctuations and climatic change*. Kluwer Academic Publishers, Dordrecht: 219–233.
- Bruland O. and Hagen J.O. 2002. Glacial mass balance of Austre Brøggerbreen (Spitsbergen) 1971–1999, modeled with a precipitation–runoff model. *Polar Research* 21: 109–121. doi: 10.3402/polar.v21i1.6477
- Ciężkowski W., Głowacki T., Grudzińska K.K., Kasza D. and Zagożdżon P.P. 2018. Front of the Werenskioldbreen (Svalbard) – Changes in Years 1957–2013. *E3S Web of Conference*: 29: 00030. doi: 10.1051/e3sconf/20182900030
- Den Ouden M., Reimer C.H. and Oerlemans J. 2008. Surface mass-balance modeling of Nordenskiöldbreen, Svalbard, Workshop on the dynamics and mass budget of Arctic glaciers/ GLACIODYN (IPY) meeting, Obergurgl, Austria.
- Grainger M. and Lister H. 1966. Wind speed, stability and eddy viscosity over melting ice surfaces. *Journal of Glaciology* 6: 101–127. doi: 10.3189/S0022143000019109
- Grabiec M., Budzik T. and Głowacki P. 2012. Modeling and Hindcasting of the Mass Balance of Werenskiöldbreen (Southern Svalbard). *Arctic, Antarctic and Alpine Research* 44: 164–179. doi: 10.1657/1938-4246-44.2.164
- Gwizdała M., Jeleńska M. and Łęczyński L. 2018. The magnetic method as a tool to investigate the Werenskiöldbreen environment (south-west Spitsbergen, Arctic Norway). *Polar Research* 37: 1–9. doi: 10.1080/17518369.2018.1436846
- Hanssen-Bauer I., Førland E.J., Hisdal H., Mayer S., Sandø A.B. and Sorteberg A. (Eds.) 2019. Climate in Svalbard 2100 - a knowledge base for climate adaptation, Norway. *Norwegian Centre of Climate Services (NCCS) for Norwegian Environment Agency (Miljødirektoratet) Report 1*. doi: 10.25607/OBP-888.
- Harding R.J. 1986. Exchanges of energy and mass associated with a melting snowpack. *Modelling Snowmelt-Induced Processes, Proceedings of the Budapest Symposium* 155: 3–15.
- Hock R. 1998. *Modelling of Glacier Melt and Discharge*. Geographisches Institut ETH, Zurich. doi: 10.3929/ethz-a-001891975
- Hock R. 2003. Temperature index melt modeling in mountains areas. *Journal of Hydrology* 282: 104–115. doi: 10.1016/S0022-1694(03)00257-9
- Hodson A.J., Anesio A.M., Tranter M., Fountain A.G., Osborn M., Prisco J., Laybourn-Parry J. and Sattler B. 2008. Glacial Ecosystems. *Ecological Monographs* 78: 41–67.
- Hodson A., Kohler J., Brinkhaus M. and Wynn P. 2005. Multi-year water and surface energy budget of a high-latitude polythermal glacier: evidence for overwinter water storage in a dynamic subglacial reservoir. *Annals of Glaciology* 42: 42–47. doi: 10.3189/172756405781812844
- Hulth J., Rolstad C., Trondsen K. and Rødby R. W. 2010. Surface mass and energy balance of Sørbreen, Jan Mayen, 2008. *Annals of Glaciology* 51: 110–119. doi: 10.3189/172756410791392754
- Ignatiuk D. 2021a. Meteorological data from the Werenskiöldbreen (Svalbard) 2009–2020 [Data set]. *Zenodo*. doi: 10.5281/zenodo.6528321
- Ignatiuk D. 2021b. Glaciological data (point mass balance, SWE, snow depth, bulk snow density, modelled runoff) from Werenskiöldbreen (Svalbard) 2009–2020 [Data set]. *Zenodo*. doi: 10.5281/zenodo.5792168
- Ignatiuk D., Piechota A., Ciepły M. and Luks B. 2015. Changes of altitudinal zones of Werenskiöldbreen and Hansbreen in period 1990–2008, Svalbard. *American Institute of Physics Conference Proceedings* 1618: 275–280. doi: 10.1063/1.4897727
- Ignatiuk D.S., Błaszczuk M., Budzik T., Grabiec M., Jania J.A., Kondracka M., Laska M., Małarzewski Ł. and Stachnik Ł. 2022. A decade of glaciological and meteorological

- observations in the Arctic (Werenskioldbreen, Svalbard). *Earth System Science Data* 14: 2487–2500. doi: 10.5194/essd-2021-464
- IPCC 2019. The Ocean and Cryosphere in a Changing Climate. <https://www.ipcc.ch/srocc/home/>, last accessed on 1 April 2020.
- Jania J. 1993. *Glaciology*. Państwowe Wydawnictwo Naukowe, Warszawa (in Polish).
- Jonsell U., Hock R. and Holmgren B. 2003. Spatial and temporal variations in albedo on Storglaciären, Sweden. *Journal of Glaciology* 49: 59–68. doi: 10.3189/172756503781830980
- Klok E. J., Nolan M. and Van Den Broeke M. 2005. Analysis of meteorological data and the surface of McCall Glacier, Alaska, USA. *Journal of Glaciology* 51: 451–461. doi: 10.3189/172756505781829241
- Klok E.J. and Oerlemans J. 2002. Model study of the spatial distribution of the energy and mass balance of Morteratschgletscher, Switzerland. *Journal of Glaciology* 48: 505–518. doi: 10.3189/172756502781831133
- Konzelmann T. and Braithwaite R.J. 1995. Variations of ablation, albedo and energy balance at the margin of the Greenland ice sheet, Kronprins Christian Land, eastern North Greenland. *Journal of Glaciology* 41: 174–182. doi: 10.3189/S002214300001786X
- Kosiba A. 1960. *Some results of glaciological investigations in SW-Spitsbergen carried out during the Polish I. G. Y. Spitsbergen Expeditions in 1957, 1958 and 1959*. Uniwersytet Wrocławski, Wrocław.
- Laska M., Luks B. and Budzik T. 2016. Influence of snowpack internal structure on snow metamorphism and melting intensity on Hansbreen, Svalbard. *Polish Polar Research* 37: 193–218. doi: 10.1515/popore-2016-0012
- Laumann T. and Reeh N. 1993. Sensitivity to climate change of the mass balance of glaciers in southern Norway. *Journal of Glaciology* 39: 656–665. doi: 10.3189/S0022143000016555
- Łepkowska E. and Stachnik Ł. 2018. Which drivers control the suspended sediment flux in a High Arctic glacierized basin (Werenskioldbreen, Spitsbergen)? *Water* 10: 1408. doi: 10.3390/W10101408
- Majchrowska E., Ignatiuk D., Jania J., Marszałek H. and Wasik M. 2015. Seasonal and interannual variability in runoff from the Werenskioldbreen catchment, Spitsbergen. *Polish Polar Research* 36: 197–224. doi: 10.1515/popore-2015-0014
- Meltofte H., Christensen T.R., Elberling B., Forchhammer M. C. and Rasch M. 2008. *High-arctic ecosystem dynamics in a changing climate, Ten years of monitoring and research at Zackenberg Research Station, Northeast Greenland*. Elsevier, Oxford. doi: 10.22621/cfn.v123i1.663
- Migała K., Piwowar B.A. and Puczko D. 2006. A meteorological study of the ablation process on Hans Glacier, SW Spitsbergen. *Polish Polar Research* 27: 243–258.
- Nuth C., Gilber, A., Köhler A., McNabb R., Schellenberger T., Sevestre H., Weidle C., Girod L., Luckman A. and Käab A. 2019. Dynamic vulnerability revealed in the collapse of an Arctic tidewater glacier. *Scientific Reports* 9: 5541. doi: 10.1038/s41598-019-41117-0
- Oerlemans J. 2000. Analysis of a 3 year meteorological record from the ablation zone of Morteratsch-gletscher, Switzerland: energy and mass balance. *Journal of Glaciology* 46: 571–579. doi: 10.3189/172756500781832657
- Ohmura A. 2001. Physical basis for the temperature-based melt-index method. *Journal of Applied Meteorology* 40: 753–761. doi: 10.1175/1520-0450(2001)040<0753:PBFTTB>2.0.CO;2
- Osuch M., Wawrzyniak T. and Łepkowska E. 2022. Changes in the flow regime of High Arctic catchments with different stages of glaciation, SW Spitsbergen. *Science of Total Environment* 817: 152924. doi: 10.1016/J.SCITOTENV.2022.152924
- Paszyński J., Miara K. and Skoczek J. 1999. Energy exchange between the atmosphere and the ground as the basis of topoclimatic mapping, *Wydawnictwo Instytutu Geografii i Przestrzennego Zagospodarowania PAN*, Warszawa (in Polish).
- Paterson W.S. 1994. *The physics of glaciers*. Butterworth Heinemann, Oxford.

- Pälli A., Moore J. C., Jania J., Kolondra L. and Głowacki P. 2003. The drainage pattern of Hansbreen and Werenskioldbreen, two polythermal glaciers in Svalbard. *Polar Research* 22: 355–371. doi: 10.1111/j.1751-8369.2003.tb00117.x
- Pereyma J., Baranowski S. and Piasecki J. 1974. Meteorological and hydrological conditions of the Werenskioldbreen and its foreground in the summer seasons of 1972 and 1973, Polska Wyprawy na Spitsbergen 1972 i 1973 r. *Materiały z Sympozjum Spitsbergeńskiego, Wrocław* (in Polish).
- Plüss C. 1997. *The energy balance over an alpine snowcover*. Geographisches Institut ETH, Zurich.
- Schuler T.V., Kohler J., Elagina N., Hagen J.O.M., Hodson A.J., Jania J.A., Kääb A.M., Luks B., Małeckı J., Moholdt G., Pohjola V.A., Sobota I. and Van Pelt, W.J. J. 2020. Reconciling Svalbard Glacier Mass Balance. *Frontiers in Earth Science* 8: 156. doi: 10.3389/FEART.2020.00156/BIBTEX
- Sevruck B. 1982. Methods of correction for systematic error in point precipitation measurement for operational use. *Operational hydrology report. World Meteorological Organization* 21: 91.
- Singh P. and Singh V.P. 2001. *Snow and glacier hydrology*. Kluwert Academic Publisher, Dordrecht, Boston, London.
- Stachniak K., Sitek S., Ignatiuk D. and Jania J. 2022. Hydrogeological model of the forefield drainage system of Werenskioldbreen, Svalbard. *Water* 14: 1514. doi: 10.3390/w14091514
- Stachnik Ł., Majchrowska E., Yde J. C., Nawrot A. P., Cichała-Kamrowska K., Ignatiuk D. and Piechota A. 2016a. Chemical denudation and the role of sulfide oxidation at Werenskioldbreen, Svalbard. *Journal of Hydrology* 538: 177–193. doi: 10.1016/J.JHYDROL.2016.03.059
- Stachnik Ł., Yde J. C., Kondracka M., Ignatiuk D. and Grzesik M. 2016b. Glacier naled evolution and relation to the subglacial drainage system based on water chemistry and GPR surveys (Werenskioldbreen, SW Svalbard). *Annals of Glaciology* 57: 19–30. doi: 10.1017/AOG.2016.9
- Stachnik Ł., Yde J. C., Krzemień K., Uzarowicz Ł., Sitek S. and Kenis P. 2022. SEM-EDS and water chemistry characteristics at the early stages of glacier recession reveal biogeochemical coupling between proglacial sediments and meltwater. *Science of the Total Environment* 835: 155383. doi: 10.1016/j.scitotenv.2022.155383.
- Sułowicz S., Bondarczuk K., Ignatiuk D., Jania J. A. and Piotrowska-Seget Z. 2020. Microbial communities from subglacial water of naled ice bodies in the forefield of Werenskioldbreen, Svalbard. *Science of the Total Environment* 723: 138025. doi: 10.1016/J.SCITOTENV.2020.138025
- Van Pelt W., Pohjola V., Pettersson R., Marchenko S., Kohler J., Luks B., Hagen J.O., Schuler T.V., Dunse T., Noël B. and Reijmer C. 2019. A long-term dataset of climatic mass balance, snow conditions, and runoff in Svalbard (1957–2018). *The Cryosphere* 13: 2259–2280. doi: 10.5194/tc-13-2259-2019
- Wawrzyniak T. and Osuch M. 2020. A 40-year High Arctic climatological dataset of the Polish Polar Station Hornsund (SW Spitsbergen, Svalbard). *Earth System Science Data* 12: 805–815. doi: 10.5194/ESSD-12-805-2020
- WGMS 2021. *Fluctuations of Glaciers Database*. World Glacier Monitoring Service, Zurich, Switzerland. doi: 10.5904/wgms-fog-2021-05
- Wheler B. A. 2004. Glacier melt modelling in the Donjek range, st. Elias Mountains. *University of Alberta*, Master thesis.
- Zhang Y., Liu S. and Ding Y. 2007. Glacier meltwater and runoff modelling, Keqıcar Baqı glacier, southwestern Tien Shan, China. *Journal of Glaciology* 53: 91–98. doi: 10.3189/172756507781833956

Received 7 June 2022

Accepted 10 October 2022